Available online at www.sciencedirect.com
SCIENCE DIRECT®
Journal of Computational Physics 198 (2004) 349–362
JOURNAL OF COMPUTATIONAL PHYSICS
www.elsevier.com/locate/jcp

# Spectral element methods on triangles and quadrilaterals: comparisons and applications

Richard Pasquetti, Francesca Rapetti *

*Laboaratory J.-A. Dieudonné, UMR CNRS 6621 and Université de Nice-Sophia Antipolis, Parc Valrose, F-06108 Nice Cedex 02, France*

Received 13 October 2003; received in revised form 15 January 2004; accepted 15 January 2004
Available online 21 February 2004

**Abstract**

In this paper, we compare a triangle based spectral element method (SEM) with the classical quadrangle based SEM and with a standard spectral method. For the sake of completeness, the triangle-SEM, making use of the Fekete points of the triangle, is first revisited. The requirement of a highly accurate quadrature rule is particularly emphasized. Then it is shown that the convergence properties of the triangle-SEM compare well with those of the classical SEM, by solving an elliptic equation with smooth (but steep) analytical solution. It is also proved numerically that the condition number grows significantly faster for triangles than for quadrilaterals. Finally, the attention is focused on a diffraction problem to show the high flexibility of the triangle-SEM.


*PACS:* 65N30; 65M60; 65M70

*Keywords:* Spectral elements; Triangular and quadrangular mesh elements; Fekete points; Gauss–Lobatto points

## 1. Introduction

The main advantage of standard spectral methods relies on the exponential convergence property as soon as smooth solutions are involved (see, e.g. [5,11,20]). The main drawback is their inability to handle complex geometries. Different strategies are, however, possible to overcome this difficulty. One of these consists in the combination of the standard spectral approximation with a penalty method [9], but the most famous one is certainly the quadrangle based spectral element method which was developed in the 80s [17,21] and then largely adopted (see, e.g. [10,16] and references herein).

However, in order to handle highly complex geometries the use of triangular (tetrahedral in 3D) elements is generally preferred. Therefore, *hp*-finite element methods have been deeply investigated during this last decade [2,6,22]. In the field of spectral methods, it was suggested to restrict the Gauss–Lobatto mesh of the

* Corresponding author.
*E-mail address:* frapetti@math1.unice.fr (F. Rapetti).

0021-9991/$ - see front matter 
doi:10.1016/j.jcp.2004.01.010

quadrilateral to the triangle [18]. Another approach was proposed in [16], based on the idea of using a change of coordinates to transform the quadrangle (and its quadrature points) into a triangle. Here, we are interested in the triangle based spectral element method (SEM) introduced in [25,26], relying on the use of Koornwinder–Dubiner polynomials [8] and Fekete points [24], and in its efficient implementation. Such an approach indeed appears to have a more valuable theoretical background.

The paper is organized as follows. To be self-contained, in Section 2 we revisit the triangle based SEM (the TSEM) using Fekete points. The convergence properties of the TSEM are investigated in Section 3, where we compare different spectral approaches, namely the standard spectral method, the standard SEM and the TSEM in terms of accuracy and efficiency. In Section 4, we use the TSEM to solve a Helmholtz problem in an open 2D domain containing a square obstacle, before going to the conclusion.

Note that we do not try to compare the SEM, the TSEM or even the usual finite element method (FEM) in terms of computational cost. Conclusions would be problem dependent, machine dependent, etc., and maybe too early to be stated. The computational cost of the usual FEM is of course inferior, but if high accuracy is desired, then spectral approaches are generally preferable, at least for smooth solutions. Moreover, in the present state of the art the standard SEM is to be preferred to the TSEM if a structured mesh can be used to discretize the computational domain, essentially due to the fact that computing derivatives is more expensive with the TSEM, as emphasized in the next section.

## 2. Triangle based SEM

Just like the SEM, the TSEM needs: (i) an orthogonal polynomial basis and (ii) a set of approximation points. In the reference square $Q = (-1,1)^2$, these two sets result from tensorial products of the Legendre polynomials and of the associated Gauss–Lobatto points, respectively.

Such a straightforward approach is no-longer possible for triangles. In the late 90s it was proposed to use Koornwinder–Dubiner (KD) polynomials to constitute an orthogonal basis in the reference triangle $T$ and Fekete points (of the triangle) as approximation points. This approach is analyzed hereafter.

### 2.1. Koornwinder–Dubiner polynomials

In the reference triangle $T = \{(r,s), 0 \geqslant r,s \geqslant -1, r+s \leqslant 0\}$, the following KD polynomials are orthonormal in $L^2(T)$, the Hilbert space of square-integrable functions on $T$ and inner product $(f,g) = \int_T f(r,s)\,g(r,s)\,\mathrm{d}r\,\mathrm{d}s$

$$\psi_{ij}(r,s) = c_{ij} P_i^{0,0}\left(\frac{2r+s+1}{1-s}\right)\left(\frac{1-s}{2}\right)^i P_j^{2i+1,0}(s), \tag{1}$$

with $c_{ij} = \sqrt{(2i+1)(i+j+1)/2}$ and $P_i^{\alpha,\beta}(x)$ being Jacobi polynomials [1].

Let us consider now the space $\mathscr{P}_N(T)$ of polynomials defined on $T$ and of total degree $\leqslant N$. KD polynomials $\psi_{ij}$, $i,j \geqslant 0$, $i+j \leqslant N$, constitute an orthonormal basis of $\mathscr{P}_N(T)$. The cardinality of this set is $n = (N+1)(N+2)/2$. Hereafter, we no-longer use the notation $\psi_{ij}$ but $\psi_k$, $1 \leqslant k \leqslant n$, with any arbitrary bijection $k \equiv k(i,j)$. In this paper, it is simply assumed that the constant polynomial is $\psi_1(r,s) = 1/\sqrt{2}$.

### 2.2. Fekete points

For a long time it has been well known that polynomial approximations of a given function, say $u$ with $u \in C^\infty(-1,1)$, are of interest only if the set of points used to set-up the approximation is well chosen. More precisely, let $P_N(-1,1)$ be the space of polynomials of maximum degree $\leqslant N$ defined in $(-1,1)$. Given a set

of points $\{x_i\}_{i=1}^{N+1}$ in $(-1,1)$, the (interpolant) polynomial $I_N u$ of $u$ at these points belongs to $P_N$ and verifies $I_N u(x_i) = u(x_i)$. The polynomial $I_N u$ and $u$ may greatly differ, i.e., $\|u - I_N u\| \gg 0$, where $\|\cdot\|$ stands for the max (uniform, $L^\infty$) norm. Legendre Gauss–Lobatto points, usually used in spectral methods, constitute a satisfactory set. Moreover, they allow for an exact quadrature of any polynomial in $P_{2N-1}$ and include boundary points, which is convenient to enforce boundary conditions. The extension of the 1D and 2D Cartesian case, with $Q$ as reference element in the frame of the SEM, is straightforward. One introduces the space $P_N(Q)$ of the polynomials defined on $Q$ of maximum degree $\leqslant N$ with respect to each variable (note that in 1D, $P_N \equiv \mathscr{P}_N$, but in 2D or 3D, $\mathscr{P}_N$ is a proper subset of $P_N$).

When non-Cartesian geometries are involved, as $T$ in the TSEM, the problem of finding a right set of points arises again. However, an essential remark is that in quadrilaterals Gauss–Lobatto points are also Fekete points [3,4] and that Fekete points may be defined in any geometry, especially in the reference triangle $T$. Given a polynomial basis, say $\{\psi_j\}_{j=1}^n$, Fekete points are those which maximize the determinant of the Vandermonde matrix $V$, whose elements are defined as $V_{ij} = \psi_j(\boldsymbol{y}_i)$, with $\boldsymbol{y}_i$, $i = 1, \ldots, n$, arbitrary points in $T$. Thus, computing Fekete points, say $\{\boldsymbol{x}_i\}_{i=1}^n$, requires to solve an optimization problem: find the set $\{\boldsymbol{x}_i\}_{i=1}^n$ of points in $T$ such that $\det(V)(\boldsymbol{x}_1, \ldots, \boldsymbol{x}_n)$ is maximal. For the triangle this problem was solved for different values of $N$, up to $N = 18$, in [24]. One may easily check that the set of Fekete points does not depend on the choice of the basis $\{\psi_j\}_{j=1}^n$ and the following important property holds [24]: Lagrange polynomials $\{\phi_j\}_{j=1}^n$ built on Fekete points, i.e., such that $\phi_j(\boldsymbol{x}_i) = \delta_{ij}$, $1 \leqslant i, j \leqslant n$, are maximal at these points. Moreover, on the sides of $T$, Fekete points coincide with Gauss–Lobatto points, allowing for conforming meshes of triangles and quadrilaterals. This was conjectured/proved in [3], numerically checked in [24] and used, e.g., in [15].

It remains that Fekete points are not Lebesgue points, i.e., points which minimize the Lebesgue constant $\|I_N\|$ appearing in the following inequality:

$$\|u - I_N u\| \leqslant (1 + \|I_N\|)\|u - u^*\|,$$

where $u^* \in \mathscr{P}_N$ is the best polynomial approximation of $u$. Fekete points are not optimal (see, e.g. [12] for better points if $N < 9$). However, one observes numerically that for Fekete points $\|I_N\| \propto N$, with the theoretical result $\|I_N\| \leqslant N$. In contrast, in the 1D case, for equidistant points the increase of the Lebesgue constant with respect to $N$ is exponential.

In Fig. 1, we compare the distributions of Fekete points, in $T$, and of Gauss–Lobatto points, in $Q$, for $N = 12$.

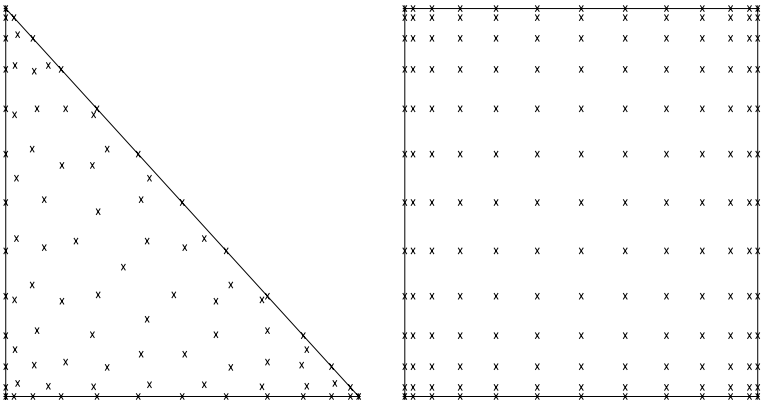

Fig. 1. Collocation points in the reference triangle (left) and square (right) for $N = 12$.

### 2.3. Derivatives and inner products

In any finite element or spectral element approximation, the key-point is to compute efficiently derivatives and inner products in each element. Let us focus on such an element, say $\omega$. As usual we introduce a mapping, say $\boldsymbol{g} : T \to \omega$ and approximate $u|_\omega \in L^2(\omega)$ with $u_N$ such that $u_N \circ \boldsymbol{g} \in \mathscr{P}_N(T)$. With $u_i$ the values of $u$ at the points $\boldsymbol{g}(\boldsymbol{x}_i)$, $u_N$ reads

$$u_N(x,y) = \sum_{i=1}^{n} u_i \phi_i(r(x,y), s(x,y)), \quad \forall (x,y) \in \omega.$$

#### 2.3.1. Derivatives

By applying the chain rule, the computation of derivatives at the approximation points yields to introduce two differentiation matrices

$$D^{\mathrm{r}}_{ij} = \partial_{\mathrm{r}} \phi_j(\boldsymbol{x}_i), \quad D^{\mathrm{s}}_{ij} = \partial_{\mathrm{s}} \phi_j(\boldsymbol{x}_i).$$

To set-up these matrices we write

$$\psi_j(\boldsymbol{x}) = \sum_{k=1}^{n} \psi_j(\boldsymbol{x}_k)\phi_k(\boldsymbol{x}) = \sum_{k=1}^{n} V_{kj}\phi_k(\boldsymbol{x}),$$

if we differentiate, e.g., with respect to $r$, and express the result at the point $\boldsymbol{x}_i$, we obtain

$$\partial_{\mathrm{r}} \psi_j(\boldsymbol{x}_i) = \sum_{k=1}^{n} V_{kj}\, \partial_{\mathrm{r}} \phi_k(\boldsymbol{x}_i) = \sum_{k=1}^{n} V_{kj} D^{\mathrm{r}}_{ik}, \quad i = 1, \ldots, n.$$

Denoting by $V^{\mathrm{r}}$ the matrix whose elements are $V^{\mathrm{r}}_{ij} = \partial_{\mathrm{r}} \psi_j(\boldsymbol{x}_i)$ and similarly for $V^{\mathrm{s}}$, in matrix form we have

$$D^{\mathrm{r}} = V^{-1} V^{\mathrm{r}}, \quad D^{\mathrm{s}} = V^{-1} V^{\mathrm{s}}.$$

Here, it should be remarked that the differentiation matrices are of dimension $n \times n$, whereas in the quadrangle based SEM they are only of dimension $(N+1) \times (N+1)$, thanks to the Cartesian structure of the mesh.

#### 2.3.2. Inner products

The usual way to approximate an integral expression as

$$I = \int_\omega uv \, \mathrm{d}\omega,$$

is to use a quadrature rule. Thus, setting $u_i = u(\boldsymbol{g}(\boldsymbol{x}_i))$, $i = 1, \ldots, n$, and similarly for $v$, and denoting by $\{w_i\}_{i=1}^n$ the set of quadrature weights and $J$ the Jacobian determinant of the mapping $\boldsymbol{g}$, we have

$$I \approx \sum_{i=1}^{n} u_i v_i J(\boldsymbol{x}_i) w_i. \tag{2}$$

Given the Fekete points, it is of course possible to compute the quadrature weights that allow for an exact calculation of any polynomial of $\mathscr{P}_N(T)$. The set of quadrature weights solves the following linear system:

$$\sum_{i=1}^{n} w_i \psi_j(\boldsymbol{x}_i) = \int_T \psi_j(\boldsymbol{x}) \, \mathrm{d}\boldsymbol{x} = \delta_{j1}, \quad j = 1, \ldots, n,$$

where the second equality results from the orthogonality of the KD polynomials. Then we simply obtain

$$w_i = \sqrt{2}(V^{-1})_{1i}.$$

This result is, however, minimal: the quadrature rule is only exact if the integrand belongs to $\mathscr{P}_N(T)$, i.e., Fekete points for the triangle fail to show the nice quadrature property of Gauss–Lobatto points for the quadrilateral. One may then check that for a second order elliptic problem as the one considered in the next section (see Eq. (4)), the exponential convergence property, characteristic of spectral methods, is lost.

A much better approximation, i.e., exact in $\mathscr{P}_{2N}$, may be obtained if $J$ is assumed constant, i.e., if $\boldsymbol{g}$ is a linear mapping [26]. In this case, denoting by $\{\hat{u}_i\}_{i=1}^n$ the spectrum of the interpolant of $u \bigcirc \boldsymbol{g}$ on the KD polynomial basis, we have

$$I \approx J\left(\sum_{i=1}^{n} \hat{u}_i\psi_i, \sum_{j=1}^{n} \hat{v}_j\psi_j\right) = J\sum_{k=1}^{n} \hat{u}_k\hat{v}_k.$$

The integral $I$ may easily be written in terms of grid-point values. From the following relations, where the superscript T stands for "transposition"

$$\begin{aligned}
&\phi_i(\boldsymbol{x}) = \sum_{j=1}^{n} V_{ij}^{-\mathrm{T}}\psi_j(\boldsymbol{x}),\\
&\hat{u}_k = \left(\sum_{i=1}^{n} u_i\phi_i, \psi_k\right) = \sum_{i=1}^{n} u_i(\phi_i, \psi_k),\\
&(\phi_i, \psi_k) = V_{ik}^{-\mathrm{T}} = V_{ki}^{-1},
\end{aligned}$$

we obtain

$$I \approx J\sum_{k=1}^{n}\left(\sum_{i=1}^{n} u_i V_{ki}^{-1}\right)\left(\sum_{j=1}^{n} v_j V_{kj}^{-1}\right) = J\sum_{i=1}^{n} u_i \sum_{j=1}^{n} v_j \sum_{k=1}^{n} V_{ki}^{-1} V_{kj}^{-1}.$$

In matrix form, with $\underline{u}$ and $\underline{v}$ gathering the $u_i$ and $v_i$, we thus have

$$I \approx J\,\underline{u}^{\mathrm{T}} W \underline{v}, \quad W = V^{-\mathrm{T}}V^{-1}. \tag{3}$$

In this paper, we only consider the case of non-deformed triangular elements, so that, being $J$ constant on each element the quadrature rule (3) is satisfactory. In case of non-linear mappings , it is relevant to use a quadrature rule based on Gauss points, showing suitable characteristics, especially symmetry, since such sets of points are known for simplices [7,23]. In this case, we should first interpolate $u$ and $v$ at the Gauss points before using a quadrature formula similar to (2).

## 3. Tests and comparisons

Our goal in this section is first to check the convergence properties of the TSEM with respect to $N$ and to the number $K$ of spectral elements. These are the so-called $p$- and $h$-convergence in the frame of $hp$-finite elements ($p$: polynomial approximation degree and $h$: space step size). Second we compare the convergence rates of different spectral approximations: the standard spectral method, the (quadrangle based) SEM and the TSEM. To this end we consider the following problem:

$$\begin{cases} -\nabla^2 u + u = f & \text{in} \quad \Omega = (-1,1)^2, \\ u = u_\Gamma & \text{on} \quad \Gamma = \partial\Omega, \end{cases} \tag{4}$$

where $f$ is the source term and $u_\Gamma$ the boundary value.

Our implementation of the spectral element method is standard (see, e.g. [16,17]). For the TSEM (as for the SEM), it may be viewed as a direct extension of the finite element method, when using for basis functions Lagrange polynomials built on Fekete points (Legendre Gauss–Lobatto points for SEM). Let us note that contrary to the SEM, the TSEM mass matrix is generally not diagonal. Thus, the elemental mass matrices are in our implementation proportional to matrix $JW$. Moreover, setting up the stiffness matrix is more costly since, as already mentioned, the dimension of the differentiation matrices corresponds to the number $n$ of Fekete points per triangle.

### 3.1. Convergence properties of the TSEM

We tested the accuracy of the TSEM by performing a $N$- and $h$-convergence study. As in [26], problem (4) is considered with the source term $f$ and the boundary value $u_\Gamma$ consistent with $u = \sin(\pi x)\sin(\pi y)$. The mesh is obtained by first dividing $\Omega$ into $K = k^2$ identical squares and then by dividing similarly each of them into two triangles. The grid-size parameter $h$ is chosen equal to $2/k$.

Fig. 2 shows the log-plots of the error for a few choices of $N$, since the zero machine (machine accuracy) is reached quite soon (for $N = 12$). As expected the convergence to the exact solution is of algebraic type and achieved with an order of accuracy equal to $(N + 1)$ with respect to $h$. Fig. 3 shows the semi log-plots of the error for a few choices of $h$. As expected exponential convergence is achieved with respect to $N$.

### 3.2. Comparison of different spectral approximations

To make a detailed comparison between the standard spectral method and the quadrangle based SEM or the TSEM, we produce now results obtained with each of these methods for the test problem (4). However, to stiffen the problem and thus avoid to reach too quickly the zero machine, the source term $f$ and the boundary value $u_\Gamma$ are here consistent with $u = \tanh 6(x^2 + y^2 - 0.5^2)$.

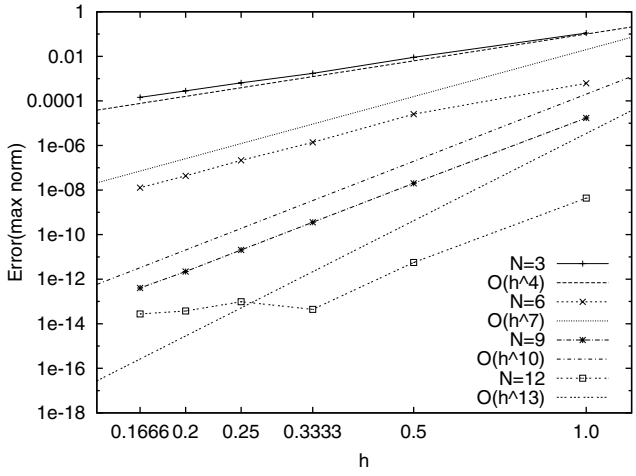


Fig. 2. A $h$-convergence study for the TSEM solution of problem (4) for different values of $N$.

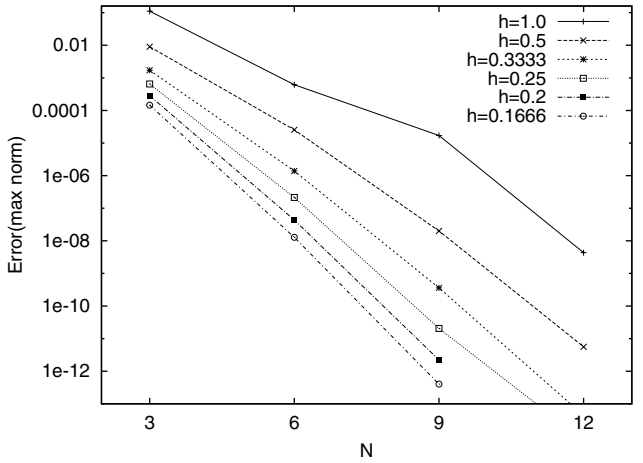


Fig. 3. A $N$-convergence study for the TSEM solution of problem (4) for different values of $h$.

Table 1
Number of grid-points for $K = k^2$ quadrangles or $K = 2k^2$ triangles with $P_N$ and $\mathscr{P}_N$ approximations, respectively

| $k/N$ | 3 | 6 | 9 | 12 | 15 | 18 |
|---|---|---|---|---|---|---|
| 2 | | 169 | 361 | 625 | 961 | 1369 |
| 4 | 169 | 625 | 1369 | 2401 | 3721 | 5329 |
| 8 | 625 | 2401 | 5329 | | | |

- For the standard spectral approach, we have used a Chebyshev collocation method, i.e., the numerical solution solves the strong form of problem (4) at the Chebyshev Gauss–Lobatto points. The polynomial space is $P_N$, i.e., the set of polynomials of maximum degree $\leqslant N$ in each variable. The following values of $N$ have been used: $N = 20, \ldots, 80$. The corresponding number of grid-points is $N_p = (N+1)^2$.
- For the SEM, the computational domain has been partitioned into $K = k^2$ identical squares, with a $P_N$ approximation in each of them. In Table 1, we give the numbers of grid-points, $N_p = (kN+1)^2$, for some choices of $k$ and $N$ among the ones we have considered while performing numerical tests. Note that, doubling $N$ or doubling $k$ yields same numbers of grid-points.
- For the TSEM, we have used $K = 2k^2$ identical triangles, obtained by dividing each square into two triangles. The polynomial space in each triangle is $\mathscr{P}_N$, i.e., the set of polynomials of total degree $\leqslant N$. The number of grid-points also equals $N_p = (kN+1)^2$.

In Figs. 4 and 5, we give the max norm of the error computed at the grid-points between the analytical solution of problem (4) and the one obtained with the SEM or the TSEM. In Fig. 4, the line associated with $k = K = 1$ corresponds to the error obtained with the standard spectral Legendre approximation of the weak form of problem (4).

Different slopes are shown for the SEM in Fig. 4 and for the TSEM in Fig. 5: they correspond, as indicated in the captions, to different choices of $k$. Each line carries points corresponding to the considered values of $N$. To make a comparison of different spectral element (SEM and TSEM) approximations, for each $k$ we made a run with values of $N$ such that $(1 + kN) < 80$. Looking at Figs. 4 and 5, we observe that for smooth problems it is better with both methods to use large values of $N$ and small $k$: the slopes which are closer to the Chebyshev approximation correspond in fact to $k = 3, 4$ and carry points for $N = 6, 9, 12,$

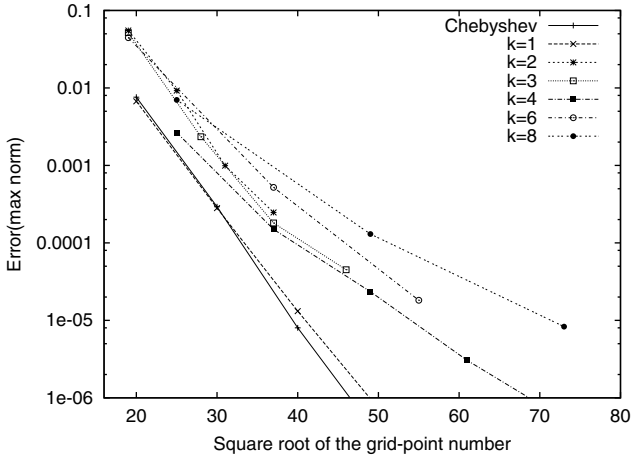


Fig. 4. Error obtained with different (related to different values of $k$) SEM approximations of problem (4), the collocation Chebyshev results being used for reference.

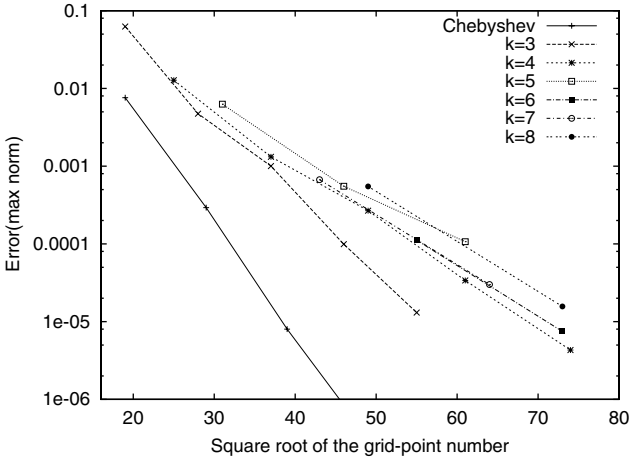


Fig. 5. Error obtained with different (related to different values of $k$) TSEM approximations of problem (4), the collocation Chebyshev results being used for reference.

15, 18. It results that the SEM and the TSEM show the exponential convergence property. In Fig. 4, it can also be remarked that the Chebyshev strong formulation approximation gives a slightly better result than the Legendre weak one. Finally, when comparing the two figures it appears that the SEM and TSEM approximations give very close results, i.e., for similar numbers $k$ of spectral elements similar accuracy may be reached with both methods.

One important aspect to consider is the condition number of the system matrix which results from the SEM or TSEM approximation of problem (4). The choice of Fekete points in case of the TSEM should find here its full justification. Fig. 6 shows the log-plot of the reciprocal of the condition number (as computed by the routine DGESVX of the LAPACK library) versus the adopted degree $N$ for both methods, the value of $k$ being fixed to 4. Clearly the condition number shows, for the SEM, a $O(N^3)$ behavior and, for the

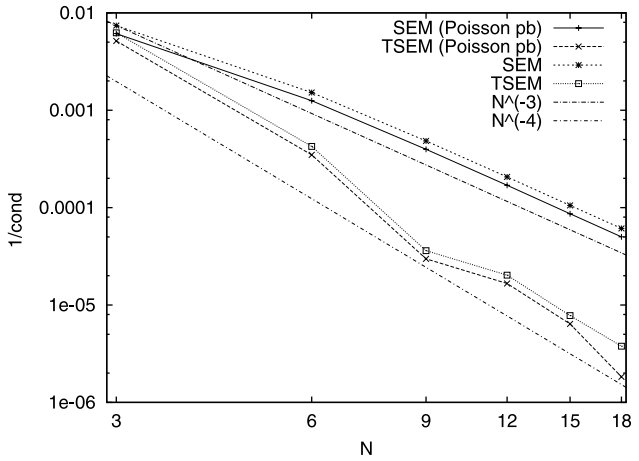


Fig. 6. Condition number of the system matrix obtained after discretization of problem (4) by the SEM or the TSEM ($k = 4$). Comparison with the condition number for the Poisson problem.

TSEM, a $O(N^4)$ one. For the SEM, the $O(N^3)$ behavior is in agreement with the theoretical result obtained in [19] (in the present study the mass matrix is the identity so that the result obtained in [19] for the stiffness matrix should be relevant). The $O(N^4)$ rather than $O(N^3)$ is more surprising and could find an explanation in the fact that the elemental mass matrix is no-longer the identity but equals $JW$ (see Eq. (3)). To verify this, we have also computed the variation of the condition number with respect to $N$ for the Poisson problem, since in this case the system matrix reduces to the stiffness matrix. The results for the Poisson problem are also presented in Fig. 6, where one remarks again the $O(N^3)$ and $O(N^4)$ behaviors of the condition number for the SEM and the TSEM, respectively.

It is worthwhile to mention that a $O(N^4)$ behavior remains acceptable. It is, e.g., the condition number for the stiffness matrix we have in 2D *hp*-finite element approximations when the usual set of hierarchical basis functions is used. In [13], it is indeed proved that for this basis the condition number should increase as $N^{4(d-1)}$, where $d$ is the space dimension.

## 4. Application to a scattering problem

Here, our goal is to apply the TSEM for the numerical resolution of a 2D scattering problem [14]. We consider a square obstacle in $\mathbb{R}^2$ intercepting a time-harmonic plane wave with constant velocity $c$, parallel to the $x$-direction. To reduce the infinite physical domain to a finite (then accessible to numerical simulations) computational domain, we introduce a non-reflecting boundary $\Gamma_T$ at a given distance $R$ from the obstacle. Due to the problem symmetry, we can study the proposed scattering problem in half domain, as shown in Fig. 7 (left), and the adopted "macromesh" is presented in Fig. 7 (right). The word "macromesh" refers to the nodes of the triangular mesh that is usually generated by a mesh generator. On each triangle of the macromesh we define Fekete nodes. The set of all Fekete nodes constitutes the "micromesh".

The wave equation in the time interval $[0, T]$, $T > 0$, writes

$$\partial_t^2 U - c^2 \nabla^2 U = 0, \qquad \text{in} \quad \Omega \times [0, T],$$

and we look for a time-harmonic (complex) solution $U$ written as the superimposition of the incident wave with the reflected/diffracted one

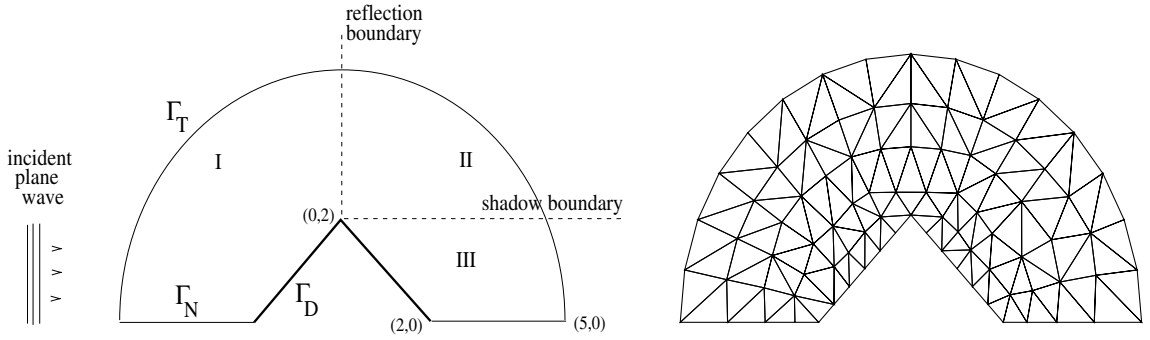


Fig. 7. Computational domain (left) and a triangular macromesh (right).

$$U = e^{i(\boldsymbol{k}\cdot\boldsymbol{x}-\omega t)} + u(\boldsymbol{x})e^{-i\omega t}.$$

Of course, only the real part of $U$ has a physical meaning.

The dispersion relation reads $|\boldsymbol{k}| = \omega/c$, so that the complex amplitude $u$ of the reflected field solves in $\Omega$ the Helmholtz equation

$$-\nabla^2 u - |\boldsymbol{k}|^2 u = 0.$$

The considered boundary conditions are defined as follows:

- Dirichlet conditions at $\Gamma_D$, the obstacle boundary: $u = -e^{i\boldsymbol{k}\cdot\boldsymbol{x}}$, so that $U = 0$.
- Homogeneous Neumann conditions at $\Gamma_N$, the axis of symmetry : $\partial_y u = 0$.
- A non-reflecting Sommerfeld radiation condition at $\Gamma_T$, the circle used to close the computational domain: $\partial_n u = i|\boldsymbol{k}|u$, where $\partial_n$ stands for the derivative in the outward normal direction. This condition minimizes the spurious reflections due to the presence of the artificial boundary.

The difficulty comes here from the fact that $u$ is a complex field. Despite the fact that the operator $\nabla^2$ is real, coupling occurs through the Dirichlet and non-reflecting boundary conditions.

Computations have been made with the following geometrical parameters: the square is of $2\sqrt{2}$ width, located at the center of the outer circle of radius $R = 5$. The wavenumber is $|\boldsymbol{k}| = 3.14$ and the wavelength $\lambda$ approximatively equals 2. In Fig. 7 (right), we show the macromesh used when $M = 6$ triangular elements match the side of the square. In this case, we approximatively have four triangles per wavelength. In contrast, at least 10 triangles per wavelength are needed with classical piece-wise linear finite elements. The results given hereafter are characterized by: (i) the polynomial approximation degree, $N$ and (ii) the number of triangles along the side of the obstacle, $M$. The computational cost directly depends on the values of these parameters, which determine the number of micromesh points.

The real part of the computed solutions in the complete domain for different values of $N$ are presented in Fig. 8. The computed solution results from the superposition of four terms: the incident and reflected geometrical optics (GO) fields and a diffracted field associated with each optical form. To better understand the computed solution, we have introduced the shadow and the reflection boundaries drawn by a dashed line in Fig. 7 (left) for the computational domain (see Fig. 9 (left) for the whole domain). GO divides the space surrounding the obstacle into well-defined regions of reflection plus direct illumination (region I), direct illumination alone (region II) and total shadow (region III). The remaining diffracted field components compensate for the discontinuities of the GO field across the two boundaries to ensure the continuity of the total field. These two boundaries are visible in Fig. 8 and, as we have represented the scattered field, we can see the field reflected from the obstacle side in region I, the field diffracted from the obstacle corners

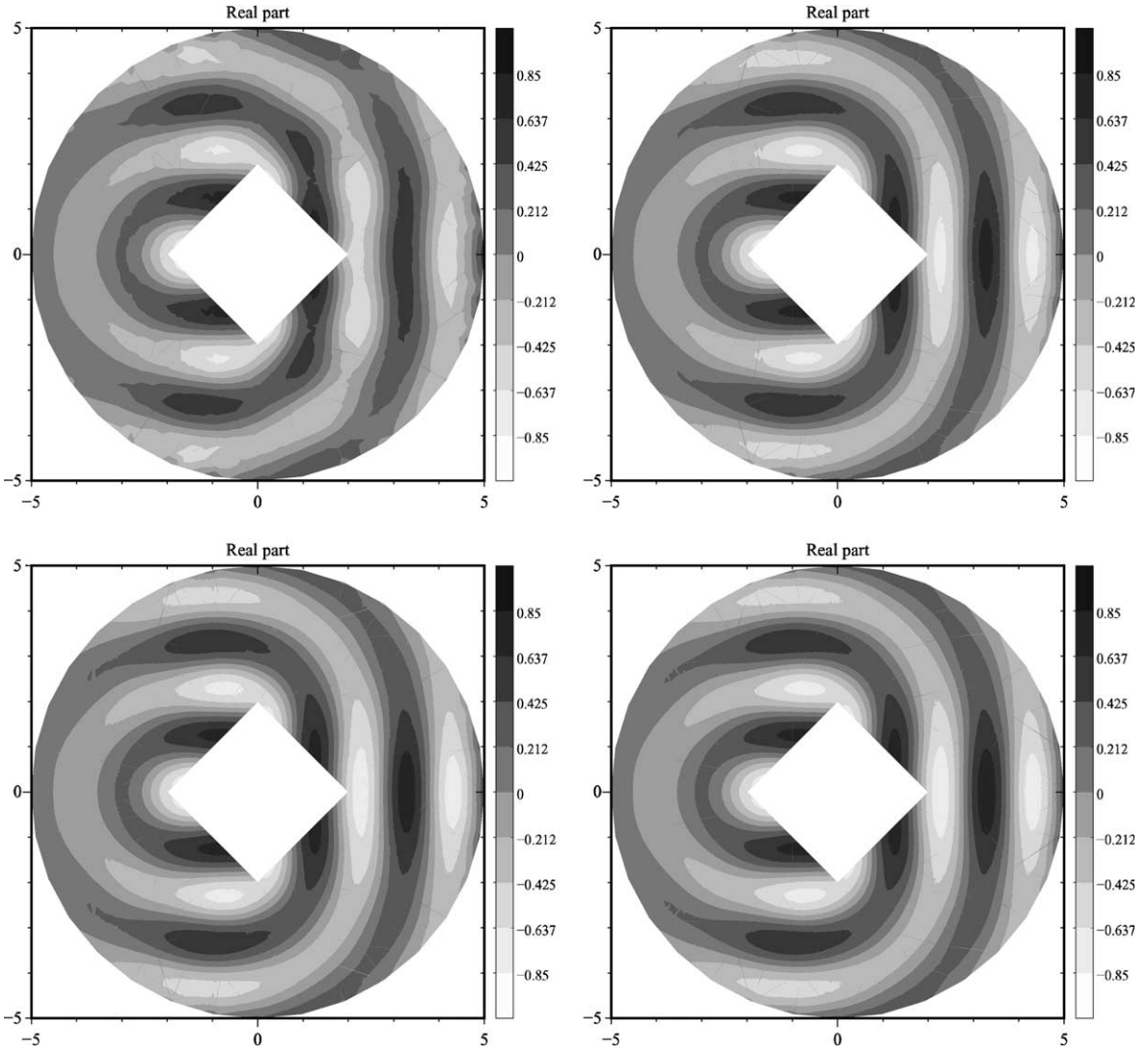


Fig. 8. Real part of the computed solution for $N = 3$ (top-left), $N = 6$ (top-right), $N = 9$ (bottom-left) and $N = 12$ (bottom-right) on a macromesh such that $M = 6$. The corresponding numbers of micromesh points are 667, 2557, 5671 and 9958, respectively.

located at (−2,0) and (0,2) (and its symmetric at (0,−2)) in regions I and II, the incident field with an opposite sign in region III.

In order to better appreciate the effect of an increase of the polynomial order $N$, let us use as "reference solution" the one obtained with $N = 15$ on the macromesh such that $M = 6$. Then one can consider some particular points and look at the error between the reference solution and the one obtained with $N < 15$ at these points. It is of interest to consider such points in the different regions, I–III, previously defined. Their coordinates are (−1.6891, 1.7902), (1.0101, 2.4069) and (2.4009, 1.2210), respectively. For the sake of simplicity, we choose such points at the vertices of the macromesh, the locations of the other collocation points depending on $N$. Fig. 9 shows the variations of the error with respect to $N$ at the chosen three points. It comes out that, as expected, the error decreases as soon as $N$ approaches $N = 15$. Moreover, the error

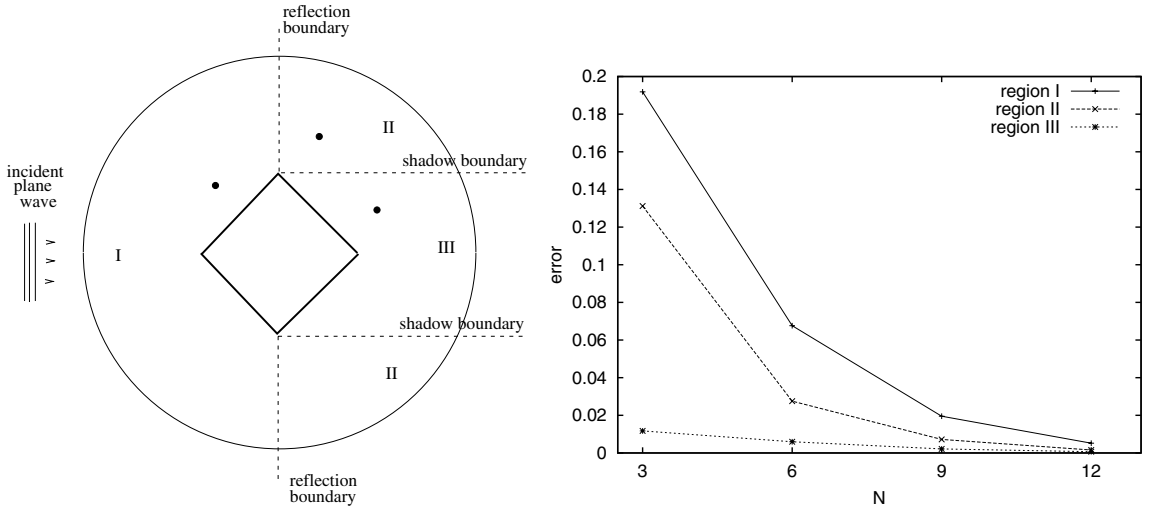


Fig. 9. Complete domain with the three points in regions I, II, III (left) and the error between the computed (reference) solution corresponding to $N = 15$ and the ones corresponding to $N = 3$, 6, 9, 12, at the given points ($M = 6$).

modulus depends on the region the particular point belongs to: in region I the scattered field is more intense than in region II or III.

To show the influence of changes in the macromesh, computations have also been done with macromeshes characterized by $M = 4$ and 8. The results obtained with the pairs ($M = 8$, $N = 6$) and ($M = 4$, $N = 9$) are shown in Fig. 10. The result obtained with ($M = 8$, $N = 6$) is already satisfactory, at least qualitatively, whereas this is not the case with ($M = 4$, $N = 9$).

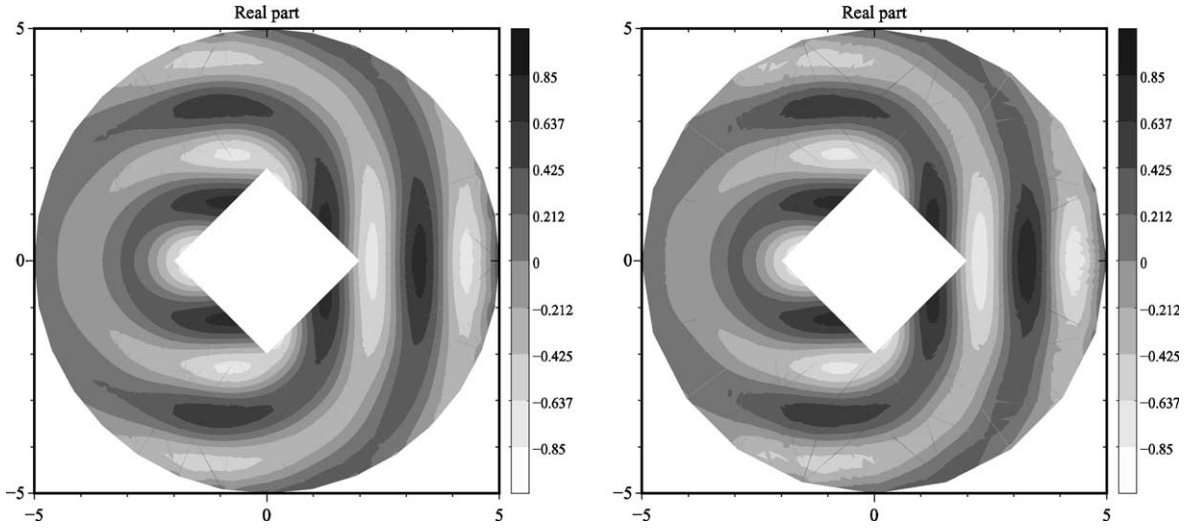


Fig. 10. Real part of the computed solution for ($N = 6$, $M = 8$) (left) and ($N = 9$, $M = 4$) (right). The corresponding numbers of micromesh points are 3037 and 2629, respectively.

To conclude with the quality of results, it is clear that the choice of the right degree $N$ to use depends on the coarseness of the macromesh as well as on the wavelength. For the given wavelength $\lambda \approx 2$, Figs. 8 and 9 show that, for the macromesh such that $M = 6$, the value $N = 3$ is too low even if the main features of the computed field are already visible. The value $N = 6$ is limit correct, better if considered on a finer mesh, as it can be noticed by comparing the results presented in Figs. 8 and 10 (left). Finally, the value $N = 9$ is limit correct for a very coarse mesh as shown in Fig. 10 (right).

## 5. Conclusions

Numerical results presented here show the capabilities of the TSEM to compute accurately solutions in highly complex geometries. The main interest, versus, e.g., *hp*-finite element methods, is that there are few changes with respect to a standard finite element approach. The presented TSEM still relies on a nodal basis and not on a modal one, i.e., the basis functions are Lagrange polynomials built on the grid-points. The gain in terms of precision is evident from the application of the method to compute the solution of test or more involved problems. When compared to the standard SEM, the main advantage of the TSEM comes from the highest capability of triangles to handle complex geometries. However, (i) for Fekete points there is no Gauss quadrature rule and (ii) the computation of the derivatives involves all collocation point values, so that the computational cost is heavier. The most natural approach will then combine the SEM with the TSEM, to get advantage of both methods' features, at least for 2D problems or 3D problems showing one periodic direction.

## Acknowledgements

We are grateful to A. Toselli (ETH, Zürich) and J.L. Guermond (LIMSI, Orsay) for fruitful discussions and we thank J.M. Lacroix, engineer of the CNRS, for his helpful technical support.

## References

[1] M. Abramowitz, I.A. Stegun (Eds.), Handbook of Mathematical Functions with Formulas Graphs and Mathematical Tables, Wiley–Interscience, New York, 1972.
[2] I. Babuska, The $p$ and $h$–$p$ versions of the finite element method: the state of the art. Finite elements. Theory and application. In: Proc. ICASE Workshop, Hampton/VA 1986, 1989, pp. 199–239.
[3] L. Bos, On certain configurations of points in $R^n$ which are uniresolvant for polynomial interpolation, J. Approx. Theory 64 (1991) 271–280.
[4] L. Bos, M.A. Taylor, B.A. Wingate, Tensor product Gauss–Lobatto points are Fekete points for the cube, Math. Comp. 70 (2001) 1543–1547.
[5] C. Canuto, M.Y. Hussaini, A. Quarteroni, T.A. Zang, Spectral Methods in Fluid Dynamics, Springer, Berlin, 1986.
[6] Q. Chen, I. Babuska, Approximate optimal points for polynomial interpolation of real functions in an interval and in a triangle, Comput. Methods Appl. Mech. Eng. 128 (1995) 485–494.
[7] R. Cools, Advances in multidimensional integration, J. Comput. Appl. Math. 149 (2002) 1–12.
[8] M. Dubiner, Spectral methods on triangles and other domains, J. Sci. Comput. 6 (1991) 345–390.
[9] M.Y. Forestier, R. Pasquetti, R. Peyret, Calculations of 3D wakes in stratified fluids, ECCOMAS Proc. Comput. Fluid Dyn. (2000).
[10] D. Funaro, Spectral Elements for Transport-dominated Equations, Springer, Berlin, 1997.
[11] D. Gottlieb, S.A. Orszag, Numerical Analysis of Spectral Methods, Theory and Applications, SIAM Publications, Philadelphia, PA, 1977.
[12] J.S. Hesthaven, From electrostatic to almost optimal nodal sets for polynomial interpolation in a simplex, SIAM J. Numer. Anal. 35 (1998) 655–676.

[13] N. Hu, X.-Z. Guo, I.N. Katz, Bounds for eigenvalues and condition number in the *p*-version of the finite element method, Math. Comp. 67 (1998) 1423–1450.
[14] J.D. Jackson, Classical Electrodynamics, Wiley, New York, 1975.
[15] D. Komatitsch, R. Martin, J. Tromp, M.A. Taylor, B.A. Wingate, Wave propagation in 2-D elastic media using a spectral element method with triangles and quadrangles, J. Comput. Acoustics 9 (2001) 703–718.
[16] G.E. Karniadakis, S.J. Sherwin, Spectral *hp* Element Methods for CFD, Oxford University Press, London, 1999.
[17] Y. Maday, A.T. Patera, Spectral element methods for the Navier–Stokes equations, in: A.K. Noor (Ed.), State-of-the-art Surveys in Computational Mechanics, ASME, New York, 1988, pp. 71–143.
[18] C. Mavriplis, J.V. Rosendale, Triangular spectral elements for incompressible fluid flow, AIAA Proc. (1993) 3346.
[19] J.M. Melenk, On condition numbers in *hp*-FEM with Gauss–Lobatto-based shape functions, J. Comput. Appl. Math. 139 (2002) 21–48.
[20] R. Peyret, Spectral Methods for Incompressible Viscous Flows, Springer, New York, 2002.
[21] E.M. Rønquist, A.T. Patera, A Legendre spectral element method for the incompressible Navier–Stokes equations, in: M. Deville (Ed.), Seventh GAMM-Conference on Numerical Methods in Fluid Mechanics Proceedings, Vieweg, Lovain-la-Neuve, Belgium, 1988, pp. 318–326.
[22] C. Schwab, *hp*-FEM for fluid flow simulation, in: T.J. Barth, H. Deconinck (Eds.), High-order Methods for Computational Physics, LNCSE 9, Springer, Berlin, 1999, pp. 325–438.
[23] A. Stroud, Approximate Calculations of Multiple Integrals, Prentice-Hall, Englewood Cliffs, NJ, 1971.
[24] M.A. Taylor, B.A. Wingate, R.E. Vincent, An algorithm for computing Fekete points in the triangle, SIAM J. Numer. Anal. 38 (2000) 1707–1720.
[25] M.A. Taylor, B.A. Wingate, A generalized diagonal mass matrix spectral element method for non-quadrilateral elements, Appl. Numer. Math. 33 (2000) 259–265.
[26] T. Warburton, L. Pavarino, J.S. Hesthaven, A pseudo-spectral scheme for the incompressible Navier–Stokes equations using unstructured nodal elements, J. Comput. Phys. 164 (2000) 1–21.